J. Quant. Spectrosc. Radiat. Transfer Vol. 34, No. 3, pp. 243–261, 1985
Printed in Great Britain.

0022–4073/85 $3.00+.00

A SYNTHETIC ACCELERATION SCHEME FOR RADIATIVE DIFFUSION CALCULATIONS

J. E. MOREL†
Simulation Theory Division, 1231, Sandia National Laboratories, Albuquerque, NM 87185, U.S.A.

E. W. LARSEN
Applied Theoretical Physics Division, Los Alamos National Laboratory, Los Alamos, NM 87545, U.S.A.

and

M. K. MATZEN
Target Iteraction Theory Division, 1265, Sandia National Laboratories, Albuquerque, NM 87185, U.S.A.

(*Received* 11 *December* 1984)

Abstract—A synthetic method has been developed to accelerate the iterative convergence of the multigroup radiative diffusion equations with temporally implicit material–radiation coupling. The performance of the method is characterized by means of a Fourier analysis. Computational results are given and are found to be consistent with the analysis. Overall, the method appears to be quite effective.

INTRODUCTION

The time-dependent material temperature and photon diffusion equations can be temporally coupled in either an explicit or implicit fashion in radiative diffusion calculations. With explicit coupling, an independent diffusion equation is obtained for each photon-energy group. Thus the explicit equations can be easily and rapidly solved. However, the explicit equations are only stable with a sufficiently small time-step. Unfortunately, the time step required for stability can become unacceptably small in the limit of strong radiation–material coupling (i.e. when the mean photon opacity is large and the material heat capacity is small). Unconditional stability can be achieved with implicit coupling, but the group diffusion equations are no longer independent. There is a common source term which makes the photon intensity for each individual group dependent upon all the other group intensities. The resulting system of equations is generally too large to be solved by direct methods even in 1-D calculations and, hence, must be solved iteratively. Unfortunately the standard iterative method becomes increasingly ineffective as the radiation–material coupling becomes stronger. Thus serious difficulties are encountered with both explicit and implicit coupling in the strong-coupling limit.

There are two common methods for dealing with these difficulties. The first method uses an approximate form of implicit coupling based upon group-dependent operator-splitting techniques. This is commonly known as the partial-temperature method.[1] An independent diffusion equation is obtained for each group intensity, and the equations are unconditionally stable, but extremely small time-steps can be required to maintain reasonable accuracy in certain types of problems. The second method accelerates the iterative convergence of the implicitly-coupled equations by means of an approximate one-group equation. This equation is obtained from the multigroup equations by means of a group-averaging process which utilizes the spectral shape of the latest solution iterate. This is the multifrequency-grey method.[1] Computational testing of this acceleration technique has so far indicated that it is quite effective, but estimating its performance for different types of problems is difficult because there has been little theoretical analysis of the method. This is a direct

†Present address: Applied Theoretical Physics Division, Los Alamos National Laboratory, Los Alamos, NM 87545, U.S.A.

consequence of the fact that the technique is nonlinear and, therefore, not amenable to standard Fourier analysis.

The purpose of this paper is to develop and test a synthetic method for accelerating the convergence of radiative diffusion calculations with implicit coupling. The synthetic method is a general acceleration method which has been extensively used in discrete-ordinates neutron transport calculations.[2-6] The standard synthetic method is a linear method, but nonlinear variants of the method are easily constructed and sometimes offer certain practical advantages over the linear scheme.[2] However, computational results obtained from discrete-ordinates applications indicate that the linear and nonlinear schemes are essentially equivalent in terms of the number of iterations required to converge the solution.[4] It is important to note that the multifrequency-grey method can be viewed as a nonlinear variant of our linear synthetic acceleration scheme. For this reason we refer to our scheme as the linear multifrequency-grey method.

The remainder of this paper is organized as follows. A general discussion is first given on synthetic acceleration methods. The equations of radiative diffusion are then given, and the standard iterative method for solving them is analyzed for a model problem. Our acceleration scheme is then developed and analyzed for the same model problem, and the connection between our scheme and the standard nonlinear multifrequency-grey technique is discussed. The complete acceleration equations are then derived for the center-differenced 1-D slab-geometry multigroup diffusion equations. Computational results are given next, followed by conclusions and recommendations for future work.

SYNTHETIC ACCELERATION METHODS

In this section we discuss the central theme of the synthetic method. We begin with a simple type of equation, which relates to a large class of numerical methods:

$$M\mathbf{x} = \mathbf{y} \quad , \tag{1}$$

where M is a linear operator, $\mathbf{x}$ is the solution vector, and $\mathbf{y}$ is the source or driving vector. We assume that M is too large to directly invert. Many standard iterative schemes are based upon a simple splitting of M into a sum of two matrices, i.e. $M = A - B$, where A can be directly inverted. This suggests the following iterative algorithm:

$$A\mathbf{x}^{l+1} = B\mathbf{x}^{l} + \mathbf{y} \quad ,$$

or equivalently

$$\mathbf{x}^{l+1} = A^{-1}B\mathbf{x}^{l} + A^{-1}\mathbf{y} \quad . \tag{2}$$

The convergence rate for this scheme is determined by the eigenvalues of the iteration operator, $A^{-1}B$. For instance, let $\{\lambda_n\}_{n=1}^{N}$ represent the eigenvalues of $A^{-1}B$. The spectral radius of $A^{-1}B$ is defined as the maximum of its eigenvalue magnitudes, i.e.

$$\mathrm{spr}(A^{-1}B) = \max\{|\lambda_n|\}_{n=1}^{N} \quad . \tag{3}$$

The error associated with the lth iterate is given by

$$\boldsymbol{\epsilon}^{l} = \mathbf{x} - \mathbf{x}^{l} \quad , \tag{4}$$

where $\mathbf{x}$ is the exact solution. It can be shown that, in the asymptotic limit of large l, successive error iterates satisfy

$$|\boldsymbol{\epsilon}^{l+1}| \leq \mathrm{spr}(A^{-1}B)\,|\boldsymbol{\epsilon}^{l}| \quad . \tag{5}$$

Thus the algorithm is convergent if the spectral radius of the iteration operator is less than unity. If the spectral radius is greater than unity, the algorithm can be expected to diverge,

although convergence can occur under extraordinary circumstances. In practice, it is found that the number of iterations required to converge the solution goes to one in the limit as the spectral radius goes to zero, and to infinity in the limit as the spectral radius goes to one.

By straightforward manipulation of Eqs. (1) and (2), the exact solution can be expressed in terms of successive iterates as follows:

$$\mathbf{x} = \mathbf{x}^{l+1} + M^{-1}B(\mathbf{x}^{l+1} - \mathbf{x}^{l}) \quad . \tag{6}$$

Equation (6) is no easier to solve than Eq. (1) because M^{-1} still appears in it. However, Eq. (6) does suggest that if a operator W can be found which is easily inverted and approximates M in some sense, then substitution of W^{-1} for M^{-1} might yield an improved approximation for $\mathbf{x}$, and thereby accelerate the convergence of the iterations. This is the central theme of the synthetic method. The operator W is called the low-order operator, and the operator M is called the high-order operator. The accelerated iterative scheme can be expressed as

$$\mathbf{x}^{l+\frac{1}{2}} = A^{-1}B\mathbf{x}^{l} + A^{-1}\mathbf{y} \quad , \tag{7a}$$

$$\mathbf{x}^{l+1} = \mathbf{x}^{l+\frac{1}{2}} + W^{-1}B(\mathbf{x}^{l+\frac{1}{2}} - \mathbf{x}^{l}) \quad . \tag{7b}$$

As one would expect, the effectiveness of this scheme depends entirely upon the choice of the low-order operator. Unfortunately, there is no general theory for making that choice, but as we shall eventually see, results from a Fourier analysis of the unaccelerated iteration scheme can be very helpful.

EQUATIONS OF RADIATIVE DIFFUSION

There are two basic equations in radiative diffusion: the material temperature equation and the radiation diffusion equation. In the Eulerian frame, they can be expressed, respectively,

$$\rho C_v \frac{\partial T}{\partial t} = \nabla \cdot K \nabla T - \nabla \cdot (\mathbf{P}\mathbf{u}) + \rho \int_0^\infty \kappa(E')[I(E') - \beta(E',T)]\, dE' + Q \quad , \tag{8}$$

$$\frac{1}{c}\frac{\partial I}{\partial t}(E) - \nabla \cdot D(E)\nabla I(E) + \rho\kappa(E)I(E) = \rho\kappa(E)\beta(E,T) \quad , \tag{9}$$

where t = time coordinate, $\mathbf{r}$ = position coordinate, E = photon energy, $C_v(\mathbf{r},T)$ = specific heat capacity [energy/(mass-temperature)], $K(\mathbf{r},T)$ = thermal conductivity [energy/(length-time-temperature)], $\mathbf{P}(r)$ = pressure tensor (material + radiation) (force/area), $\mathbf{u}(\mathbf{r})$ = material velocity (length/time), $\rho(\mathbf{r})$ = material density (mass/volume), $\kappa(\mathbf{r},E,T)$ = mass absorption opacity (area/mass), $D(\mathbf{r},E,T)$ = photon diffusion coefficient (length), $T(\mathbf{r},t)$ = material temperature, $I(\mathbf{r},E,t)$ = photon intensity [energy/(area-time)], β(E,T) = Planck function = $(8\pi E^3/h^2c)\{\exp(E/kT)-1\}^{-1}$ [energy/(area-time)], $Q(t)$ = material energy source [energy/(volume-time)]. The multigroup approximation to Eq. (9) is obtained by partitioning the energy domain into a set of intervals called groups and successively integrating the equation over each group.[7] Performing this partition, Eqs. (8) and (9) become

$$\rho C_v \frac{\partial T}{\partial t} = \nabla \cdot K \nabla T - \nabla \cdot (\mathbf{P}\mathbf{u}) + \rho \sum_{g=1}^{NG} \kappa_g[I_g - \beta_g(T)] + Q \quad , \tag{10}$$

$$\frac{1}{c}\frac{\partial I_k}{\partial t} - \nabla \cdot \mathbf{D}_k \nabla I_k + \rho\kappa_k I_k = \rho\kappa_k\beta_k(T), \quad k = 1,NG \quad , \tag{11}$$

where

$$I_k = \int_{E_{k+\frac{1}{2}}}^{E_{k-\frac{1}{2}}} I(E')\, dE' \quad , \tag{11a}$$

$$\beta_k = \int_{E_{k-\frac{1}{2}}}^{E_{k-\frac{1}{2}}} \beta(E')\,dE' \quad , \tag{11b}$$

$$\mathbf{D}_k \nabla I_k = \int_{E_{k+\frac{1}{2}}}^{E_{k-\frac{1}{2}}} D(E') \nabla I(E')\,dE' \quad , \tag{11c}$$

$$\kappa_k = \left\{ \int_{E_{k-\frac{1}{2}}}^{E_{k-\frac{1}{2}}} \kappa(E')[\beta(E') - I(E')]\,dE' \right\} / \left\{ \int_{E_{k+\frac{1}{2}}}^{E_{k-\frac{1}{2}}} [\beta(E') - I(E')]\,dE' \right\} \quad , \tag{11d}$$

$E_{k-\frac{1}{2}}$ and $E_{k+\frac{1}{2}}$ denote the upper and lower energy bounds, for the kth group, respectively, and NG is the total number of groups. The groups are contiguous, so $E_{k-\frac{1}{2}}$ is the lower bound for group $k+1$. It is important to note that the multigroup method is exact if the group-averaged quantities given by Eqs. (11c) and (11d) can be exactly evaluated. However, this is almost never possible since knowledge of the intensity function shape within each group is required. Nonetheless, in the limit as the number of groups is increased, the variation of $D(E)$ and $\kappa(E)$ within each group decreases, and the group-averaged values correctly converge regardless of the assumed intensity shape. Some sort of asymptotic solution is generally used to obtain an intensity shape for the group-averaging process. For instance, Rosseland-averaging is exact in the optically-thick limit, while Planck-averaging is exact in the optically-thin limit.[7]

In order to insure stability, we would like to use a straightforward implicit temporal differencing scheme for Eqs. (10) and (11), viz.

$$\frac{\rho C_v^{n+1}}{\Delta t}(T^{n+1} - T^n) = \nabla \cdot K^{n+1} \nabla T^{n+1} - \nabla \cdot (\mathbf{Pu}) + \rho \sum_{g=1}^{NG} \kappa_g^{n+1} [I_g^{n+1} - \beta_g^{n+1}] + Q^{n+1} \quad , \tag{12}$$

$$\frac{1}{c\Delta t}(I_k^{n+1} - I_k^n) - \nabla \cdot \mathbf{D}_k^{n+1} \nabla I_k^{n+1} + \rho \kappa_k^{n+1} I_k^{n+1} = \rho \kappa_k^{n+1} \beta_k^{n+1}, \quad k = 1, NG \quad , \tag{13}$$

where n is the time-step index. The pressure, material velocity and density are assumed to be known since they are obtained at each time-step from the hydrodynamic (conservation of mass and momentum) equations. Equations (12) and (13) are difficult to solve in their present form for two reasons: First, such quantities as C_v, κ and β are nonlinear functions of temperature, and second, the coupling between the temperature and radiation equations is nonlocal due to the presence of the thermal conductivity term. The significance of this latter fact will eventually be made clear.

In order to deal with these difficulties, we make several modifications to Eqs. (12) and (13). First, the heat capacity, diffusion coefficient and opacity values at t^{n+1} are replaced with values at t^n. This greatly simplifies the equations without any noticeable decrease in stability [assuming a standard time-step restriction which insures small relative changes in temperature over a single time-step—e.g. see Eq. (19)]. Second, time-advanced values for the Planck function are retained, but they are evaluated in terms of a first-order Taylor-series expansion. Finally, the coupling between the temperature and radiation equations is made local by means of an operator-splitting procedure. This amounts to nothing more than calculating two temperature changes: one due to the radiation and inhomogeneous source terms, and the other due to the thermal conductivity and pressure terms. Specifically, the modified equations take the form

$$\rho \frac{C_v^n}{\Delta t} \Delta T^{n+\frac{1}{2}} = \rho \sum_{g=1}^{NG} \kappa_g^n \left[I_g^{n+1} - \left(\beta_g^n + \frac{\partial \beta_g^n}{\partial T} \Delta T^{n+\frac{1}{2}} \right) \right] + Q^{n+1} \quad , \tag{14}$$

$$\frac{1}{c\Delta t}(I_k^{n+1} - I_k^n) - \nabla \cdot \mathbf{D}_k^n \nabla I_k^{n+1} + \rho \kappa_k^n I_k^{n+1} = \rho \kappa_k^n \left(\beta_k^n + \frac{\partial \beta_k^n}{\partial T} \Delta T^{n+\frac{1}{2}} \right), \quad k = 1, NG \quad , \tag{15}$$

$$\rho\frac{C_v^n}{\Delta T}\Delta T^{n+1} = \nabla\cdot K^n\nabla T^{n+1} - \nabla\cdot(\mathbf{Pu}) \quad , \tag{16}$$

where

$$T^{n+\frac{1}{2}} = T^n + \Delta T^{n+\frac{1}{2}} \quad \& \quad T^{n+1} = T^{n+\frac{1}{2}} + \Delta T^{n+1} \quad . \tag{16a}$$

It is important to note that $T^{n+\frac{1}{2}}$ does not represent the temperature at some intermediate time $t^{n+\frac{1}{2}}$, but rather represents an intermediate value for the temperature at t^{n+1}. The importance of the operator split is that it allows the temperature dependence to be eliminated from the multigroup diffusion equation. In particular, Eq. (14) can be used to solve for

$$\Delta T^{n+\frac{1}{2}} = \left[\sum_{g=1}^{NG}\kappa_g^n\left(I_g^{n+1} - \beta_g^n\right) + \frac{Q^{n+1}}{\rho}\right]\Big/\left[\frac{C_v^n}{\Delta t} + \sum_{g=1}^{NG}\kappa_g^n\frac{\partial\beta_g^n}{\partial T}\right] \quad . \tag{17}$$

Substituting Eq. (17) into Eq. (15) yields the final form of the multigroup diffusion equation

$$\frac{1}{c\Delta t}(I_k^{n+1} - I_k^n) - \nabla\cdot\mathbf{D}_k\nabla I^{n+1} + \rho\kappa_k I_k^{n+1} = \eta\chi_k\rho\sum_{g=1}^{NG}\kappa_g I_g^{n+1} + q_k, \quad k = 1,NG \quad , \tag{18}$$

where

$$\eta = \left[\sum_{g=1}^{NG}\kappa_g\frac{\partial\beta_g}{\partial T}\right]\Big/\left[\frac{C_v}{\Delta t} + \sum_{g=1}^{NG}\kappa_g\frac{\partial\beta_g}{\partial T}\right] \quad , \tag{18a}$$

$$\chi_k = \left[\kappa_k\frac{\partial\beta_k}{\partial T}\right]\Big/\left[\sum_{g=1}^{NG}\kappa_g\frac{\partial\beta_g}{\partial T}\right] \quad , \tag{18b}$$

$$q_k = \rho\kappa_k\beta_k + \eta\chi_k\left[Q - \rho\sum_{g=1}^{NG}\kappa_g\beta_g\right] \quad . \tag{18c}$$

The time index n has been supressed for all quantities except the intensities in Eqs. (18) through (18c). Equations (16)–(18) represent a linearized approximation to Eqs. (12) and (13). The solution sequence is as follows. Equation (18) is solved for the intensities. The intensities are then substituted into Eq. (17) to solve for $\Delta T^{n+\frac{1}{2}}$. Finally, Eq. (16) is solved for ΔT^{n+1}, and the two temperature changes are summed to obtain the total change.

It is clear that the operator-splitting procedure greatly simplifies the coupling between the radiation and temperature equations, but it is not obvious as to its effect on accuracy. In general, operator splitting can be expected to yield significant error whenever the calculated temperature changes are large and opposite in sign. If splitting were not used, accuracy would generally be maintained by restricting the time step such that

$$|T^{n+1} - T^n| < \alpha T^n \quad , \tag{19}$$

where α is on the order of 0.05. With the splitting which we have performed, accuracy can be maintained by using Eq. (19) in conjunction with the two restrictions

$$|\Delta T^{n+\frac{1}{2}}| < \alpha T^n \quad , \tag{19a}$$

$$|\Delta T^{n+1}| < \alpha T^n \quad . \tag{19b}$$

If both temperature changes have the same sign, the time step will be determined by Eq. (19), whereas if the signs differ, the time step will be determined by either Eq. (19a) or Eq. (19b). This procedure seems to work quite well. If it were to fail, it would do so by requiring excessively small time-steps, but we have never observed such a failure. It is important that the reader not confuse our operator-splitting technique with the partial-temperature method referred to in the introductory section of this paper. Although we do obtain partial-tem-

perature changes, the partial-temperature method involves group-dependent splitting in addition to that which we have done. It is this additional splitting which leads to the difficulties associated with the partial-temperature method.

STANDARD ITERATIVE SOLUTION OF THE DIFFUSION EQUATION

It is convenient for our purposes to write Eq. (18) as

$$-\nabla \cdot \mathbf{D}_k \nabla I_k + (\sigma_a + \sigma_{f,k}) I_k = \eta \chi_k \sum_{g=1}^{NG} \sigma_{f,g} I_g + S_k, \quad k = 1,NG \quad , \tag{20}$$

where

$$\sigma_a = 1/c\Delta t \quad , \tag{20a}$$

$$\sigma_{f,k} = \rho \kappa_k \quad , \tag{20b}$$

$$S_k = q_k + I_k^{\eta}/c\Delta t \quad . \tag{20c}$$

From Eq. (20), it can be seen that the time-dependent radiative diffusion equation which we seek to solve is equivalent to a steady-state neutron diffusion equation. The absorption opacity is equivalent to a fission cross-section. The time derivative gives rise to an effective absorption cross-section and also contributes to the inhomogeneous source. The effective fission spectrum is given by χ_k, and the number of neutrons per fission is given by η. This analogy is both interesting and useful in that it allows us to interpret the effect of each term in the equation in terms of the physical process of neutron diffusion with fission. In addition, numerical methods for solving the neutron diffusion equation can be directly applied to the radiative diffusion equation, and vice versa. This is clearly desirable since numerical methods for solving the neutron diffusion equation are well developed.

In reality, η relates to the fraction of the photon energy absorbed during a time step which is re-emitted during that same step. Inspection of Eq. (18a) shows that this fraction is always less than one, but can be arbitrarily close to one.

This multigroup diffusion equation is difficult to solve directly because of the full coupling which occurs between groups through the "fission" or re-emission source. The standard procedure for solving Eq. (20) is to avoid this coupling simply by iterating on the re-emission source. Specifically

$$-\nabla \cdot \mathbf{D}_k \nabla I_k^{l+1} + (\sigma_a + \sigma_{f,k}) I_k^{l+1} = \eta \chi_k \sum_{g=1}^{NG} \sigma_{f,g} I_g^{l} + S_k, \quad k = 1,NG \quad , \tag{21}$$

where l is the iteration index. It can be seen from Eq. (21) that performing one iteration is equivalent to solving NG independent diffusion equations.

The effectivness of this iterative scheme can be investigated by means of a standard Fourier analysis. We begin by considering an infinite one-dimensional slab geometry with spatially independent coefficients (i.e. opacities, etc.). A spatial dependence of the following form is assumed for the intensities and the source, respectively:

$$I_g(x) = I_g e^{j\lambda x}, \quad S_g(x) = S_g e^{j\lambda x}, \quad j^2 = -1, \quad -\infty < \lambda < \infty \quad . \tag{22}$$

Substituting Eq. (22) into Eq. (21) gives

$$I_k^{l} = [(\eta \chi_k \sum_{g=1}^{NG} \sigma_{f,g} I^{l-1}_{g}) + S_k]/[D_k \lambda^2 + \sigma_a + \sigma_{f,k}] \quad . \tag{23}$$

The exact solution satisfies

$$I_k = [(\eta \chi_k \sum_{g=1}^{NG} \sigma_{f,g} I_g) + S_k]/[D_k \lambda^2 + \sigma_a + \sigma_{f,k}] \quad . \tag{24}$$

By substracting Eq. (24) from Eq. (23), we obtain the relation between successive iterate intensity errors

$$\epsilon_k^{l+1} = [\eta\chi_k \sum_{g=1}^{NG} \sigma_{f,g}\epsilon_g^l]/[D_k\lambda^2 + \sigma_a + \sigma_{f,k}] \quad , \tag{25}$$

where

$$\epsilon_k^l = I_k - I_k^l \quad . \tag{25a}$$

Evaluating the ratio of successive intensity errors gives

$$(\epsilon_k^{l+1}/\epsilon_k^l) = (f^l/f^{l-1}) \quad , \tag{26}$$

where

$$f = \sum_{g=1}^{NG} \sigma_{f,g}\epsilon_g \quad . \tag{26a}$$

We refer to f as the re-emission source error. It is clear from Eq. (26) that the intensities and the source converge at the same rate. Multiplying Eq. (25) by $\sigma_{f,k}$ and summing over all groups relates successive source errors by

$$f^{l+1} = \omega(\lambda) f^l \quad , \tag{27}$$

where

$$f^l = \sum_{g=1}^{NG} \sigma_{f,g}(\epsilon_g - \epsilon_g^l) \quad , \tag{27a}$$

$$\omega(\lambda) = \eta \sum_{g=1}^{NG} [\chi_g\sigma_{f,g}]/[D_g\lambda^2 + \sigma_a + \sigma_{f,g}] \quad . \tag{27b}$$

It can be seen from Eq. (27) that $\omega(\lambda)$ is the source iteration eigenvalue for the Fourier mode corresponding to λ. Inspection of Eq. (27b) shows that $\omega(\lambda)$ is positive and a monotonically decreasing function of λ^2. Thus the spectral radius is given by the eigenvalue at $\lambda = 0$. Specifically

$$\text{spr} = \eta \sum_{g=1}^{NG} [\chi_g\sigma_{f,g}]/[\sigma_a + \sigma_{f,g}] \quad . \tag{28}$$

It can be seen from Eqs. (18a) and (20a) that η approaches unity and σ_a approaches zero in the limit as the time step is increased. Inspection of Eq. (28) shows that the spectral radius goes to unity under these same conditions. Furthermore, in practice one finds that σ_a is generally much less than $\sigma_{f,g}$ with typical time-steps, so that the spectral radius is essentially equal to η. In the strong radiation–material coupling limit (i.e. small heat capacity and large opacity), η goes to unity. Thus our analysis clearly shows that the spectral radius for the standard or unaccelerated algorithm can become arbitrarily close to unity either with large time-steps or with strong radiation–material coupling.

It is appropriate to ask what this analytic result means in terms of the convergence rate observed in realistic calculations. Our analysis applies to an infinite medium, whereas realistic calculations are always done for a finite medium. In practice, the convergence rate is found to improve as the system size (measured in terms of optical depth) decreases, but as one would expect, the convergence rate approaches that for an infinite-medium calculation as the system size increases. This dependence on system size occurs primarily because all Fourier modes are not present in a finite-medium calculation. In particular, the modes

corresponding to values of λ satisfying $|\lambda| < |\lambda|_{min}$, where $|\lambda|_{min}$ increases with decreasing system size, are absent. Since the modes corresponding to "small" values of λ are the most slowly convergent, the convergence rate is improved. Thus an infinite-medium spectral radius-of-unity means that both arbitrarily slow and arbitrarily rapid convergence rates can be observed in realistic finite-medium calculations, depending upon the size of the system. Problems with optically-thick regions, and thus slow convergence rates, are quite common.

It can be seen from Eq. (28) that the spectral radius becomes arbitrarily small with a sufficiently small time-step. This would suggest that one might simply use a sufficiently small time-step to obtain rapid convergence. However, in practice one finds that this is not an effective strategy. Although the number of iterations per time step decreases, the total number of times steps required to complete the calculation increases, resulting in inordinately long running times coupled with the threat of accumulated truncation error due to the use of extremely small time-steps.

In order to demonstrate the dependence of the eigenvalue as a function of λ, Eq. (27b) is plotted in Fig. 1 for the case of an infinite time-step (i.e. $\sigma_a = 0.0$, $\eta = 1.0$). The opacities used for this plot are taken from a 33-group set collapsed from the Los Alamos Astrophysical Library[8] using Rosseland-averaging, and correspond to iron at one-tenth standard density and a temperature of 100 eV. The diffusion coefficients are a direct function of the opacities (see next paragraph). These opacities are used throughout this paper as model opacities. We have chosen these particular opacities only because they are realistic for a material of moderate atomic number at a moderate temperature and density.

The opacities are given in Table 1. With Rosseland-averaging, the multigroup diffusion tensor reduces to a scalar diffusion coefficient. The coefficients are simply given by $D_g = [3(\sigma_{fg} + \sigma_{sg})]^{-1}$ where σ_{fg} and σ_{sg} denote the absorption and scattering opacities, respectively. It should be noted that the opacities for the first (lowest energy) group were given as "infinite" in the original tables because the mean group frequency lies below the material plasma frequency. Since "infinite" values are numerically unacceptable, we have simply used the values from the second group. Our results are essentially insensitive to the values used, since very little energy is emitted in the first group at a temperature of 100 eV.

THE ACCELERATED ITERATION ALGORITHM

As previously noted, the effectiveness of the synthetic acceleration approach is entirely dependent upon the choice of the low-order operator. In the general case, it is often not obvious as to how one should either find or go about developing such an operator. However, in a preliminary development of our method, Larsen proposed a simple strategy for developing the low-order operator which has proven to be quite effective.[9] It is based upon information from the Fourier analysis of the unaccelerated iteration scheme. In particular,

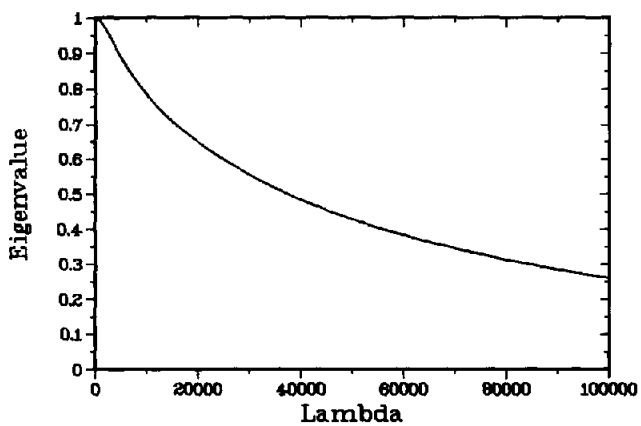

Fig. 1. Plot of unaccelerated eigenvalues for an infinite time-step.

Table 1. Rosseland-averaged multigroup opacities for iron at a density of 0.789 g/cm³ and a temperature of 100 eV.

Group Bounds (eV)	Absorption Opacity (cm^2/g)	Total Opacity (cm^2/g)
1.0 E-2 - 1.8 E0	4.9 E4	4.9 E4
1.8 E0 - 3.2 E1	4.9 E4	4.9 E4
3.2 E1 - 5.6 E1	3.5 E4	3.5 E4
5.6 E1 - 7.5 E1	2.6 E4	2.6 E4
7.5 E1 - 1.0 E2	6.6 E4	6.6 E4
1.0 E2 - 1.3 E2	1.0 E5	1.0 E5
1.3 E2 - 1.8 E2	5.1 E4	5.1 E4
1.8 E2 - 2.4 E2	2.2 E4	2.2 E4
2.4 E2 - 3.2 E2	1.4 E4	1.4 E4
3.2 E2 - 4.2 E2	4.8 E3	4.8 E3
4.2 E2 - 5.6 E2	2.8 E3	2.8 E3
5.6 E2 - 7.5 E2	1.6 E3	1.6 E3
7.5 E2 - 1.0 E3	5.5 E3	5.5 E3
1.0 E3 - 1.3 E3	4.0 E3	4.0 E3
1.3 E3 - 1.8 E3	2.1 E3	2.1 E3
1.8 E3 - 2.4 E3	1.1 E3	1.1 E3
2.4 E3 - 3.2 E3	5.6 E2	5.6 E2
3.2 E3 - 4.2 E3	2.8 E2	2.8 E2
4.2 E3 - 5.6 E3	1.4 E2	1.4 E2
5.6 E3 - 7.5 E3	6.6 E1	6.6 E1
7.5 E3 - 1.0 E4	3.5 E2	3.5 E2
1.0 E4 - 1.3 E4	1.7 E2	1.7 E2
1.3 E4 - 1.8 E4	7.7 E1	7.7 E1
1.8 E4 - 2.4 E4	3.5 E1	3.5 E1
2.4 E4 - 3.2 E4	1.5 E1	1.5 E1
3.2 E4 - 4.2 E4	6.5 E0	6.6 E0
4.2 E4 - 5.6 E4	2.8 E0	2.9 E0
5.6 E4 - 7.5 E4	1.2 E0	1.3 E0
7.5 E4 - 1.0 E5	5.0 E-1	6.1 E-1
1.0 E5 - 1.3 E5	2.2 E-1	3.4 E-1
1.3 E5 - 1.8 E5	8.3 E-2	2.0 E-1
1.8 E5 - 2.4 E5	3.4 E-2	1.5 E-1
2.4 E5 - 3.0 E5	1.4 E-2	1.3 E-1

the analysis shows that the largest eigenvalues occur in the region about $\lambda = 0$. This suggests that the convergence would be improved if a low-order operator could be found which closely approximates the high-order operator in the limit as λ approaches zero. This is not difficult to do since this limit corresponds to the spatially-constant or equilibrium limit. For instance, from Eqs. (6) and (20) it follows that the exact equation for the intensity error after the lth iteration is

$$-\nabla \cdot \mathbf{D}_k \nabla \epsilon_k^l + (\sigma_a + \sigma_{f,k})\epsilon_k^l = \eta \chi_k \sum_{g=1}^{NG} \sigma_{f,g}[\epsilon_g^l + I_g^l - I_g^{l-1}], \quad k = 1,NG \quad . \tag{29}$$

In the equilibrium limit, the gradient term goes to zero and the solution to Eq. (29) is

$$\epsilon_k = \eta(\chi_k/\sigma_{t,k})(\xi^l + r^l) \quad , \tag{30}$$

where

$$r^l = \sum_{g=1}^{NG} \sigma_{f,g}(I_g^l - I_g^{l-1}) \quad , \tag{30a}$$

$$\sigma_{t,k} = \sigma_a + \sigma_{f,k} \quad , \tag{30b}$$

$$\xi^l = \eta r^l \langle \sigma_f \rangle / (\langle \sigma_t \rangle - \eta \langle \sigma_f \rangle) \quad , \tag{30c}$$

$$\langle \sigma_t \rangle = \left[\sum_{g=1}^{NG} (\chi_g / \sigma_{t,g}) \right]^{-1} \quad , \tag{30d}$$

$$\langle \sigma_f \rangle = \langle \sigma_t \rangle \sum_{g=1}^{NG} (\chi_g \sigma_{f,g} / \sigma_{t,g}) \quad . \tag{30e}$$

For our purpose, the most important characteristic of the equilibrium solution is its spectral shape. From Eqs. (30) and (30d), it follows that the normalized spectrum is

$$\langle \sigma_t \rangle \chi_k / \sigma_{t,k} \quad . \tag{31}$$

It may be confusing that Eq. (31) does not represent a Planckian spectrum. However, it must be remembered that Eq. (30) relates to the intensity error rather than the intensity itself. Although the equilibrium intensity spectrum is Planckian, the equilibrium spectrum of the intensity error is not. In the limit as Δt goes to infinity, the spectrum given by Eq. (31) is the multigroup-equivalent of the spectrum used to obtain Rosseland-mean opacities.

We can obtain a one-group equation from the multigroup equation in a manner completely analogous to that by which the multigroup equation is obtained from the continuous-energy equation. Just as the multigroup equation produces the exact continuous-energy solution if the spectral shape is known within each group, the one-group equation produces the exact multigroup solution if the global spectral shape is known. Although we do not know the multigroup spectrum for the general case, we do know it for the equilibrium case. Thus, if we use the equilibrium spectrum to derive a one-group equation, we can expect the one-group solution to be exact in the equilibrium limit.

The one-group equation is derived as follows. We first assume that the multigroup spectrum is given by the equilibrium spectrum, i.e.

$$\epsilon_k^l = E^l \langle \sigma_t \rangle \chi_k / \sigma_{t,k}, \quad k = 1,NG \quad . \tag{32}$$

Equation (29) is then summed over all groups. The result is

$$-\nabla \cdot [\langle \mathbf{D} \rangle \nabla E^l + \langle \mathbf{D}' \rangle E^l] + [\sigma_a + (1 - \eta)\langle \sigma_f \rangle] E^l = \eta r^l \quad , \tag{33}$$

where

$$\langle \mathbf{D} \rangle = \langle \sigma_t \rangle \sum_{g=1}^{NG} (\chi_g \mathbf{D}_g / \sigma_{t,g}) \quad , \tag{33a}$$

$$\langle \mathbf{D}' \rangle = \sum_{g=1}^{NG} \mathbf{D}_g \nabla [\langle \sigma_t \rangle (\chi_g / \sigma_{t,k})] \quad . \tag{33b}$$

The one-group operator defined by Eq. (33) constitutes the low-order operator in our synthetic acceleration scheme. Such an equation can be directly solved using Gaussian elimination in 1-D, and efficiently solved in 2-D using standard iterative methods.

Following Eqs. (7a) and (7b), the accelerated algorithm can be expressed as

$$-\nabla \cdot \mathbf{D}_k \nabla I_k^{l+\frac{1}{2}} + (\sigma_a + \sigma_{f,k}) I_k^{l+\frac{1}{2}} = \eta \chi_k \sum_{g=1}^{NG} \sigma_{f,g} I_g^l + S_k, \quad k = 1,NG \quad , \tag{34a}$$

$$-\nabla \cdot [\langle \mathbf{D} \rangle \nabla E^{l+\frac{1}{2}} + \langle \mathbf{D}' \rangle E^{l+\frac{1}{2}}] + [\sigma_a + (1 - \eta)\langle \sigma_f \rangle] E^{l+\frac{1}{2}} = \eta r^{l+\frac{1}{2}} \quad , \tag{34b}$$

$$I_k^{l+1} = I_k^{l+\frac{1}{2}} + E^{l+\frac{1}{2}} \langle \sigma_t \rangle \chi_k / \sigma_{t,k}, \quad k = 1,NG \quad . \tag{34c}$$

where

$$r^{l+\frac{1}{2}} = \sum_{g=1}^{NG} \sigma_{fg}(I_g^{l+\frac{1}{2}} - I_g^l) \quad . \tag{34d}$$

The Fourier analysis for the accelerated scheme is a straightforward extension of the analysis for the unaccelerated scheme; thus we omit the details. The resulting expression for the eigenvalue is

$$\omega_a(\lambda) = \omega_u(\lambda) + [\omega_u(\lambda) - 1.0]\langle\sigma_f\rangle/[\langle D\rangle\lambda^2 + \sigma_a + (1 - \eta)\langle\sigma_f\rangle] \quad , \tag{35}$$

where ω_u denotes the eigenvalue for the unaccelerated scheme, which is given by Eq. (27b). The spectral radius corresponding to Eq. (35) must be obtained computationally since we have not been able to derive a closed-form expression for it. Both the unaccelerated and accelerated eigenvalues are plotted as a function of λ in Fig. 2 for an infinite time-step and using the model opacities. The accelerated spectral radius is approximately 0.57 as compared with the unaccelerated value of unity. A similar plot is given in Fig. 3 for a time step of 5.0×10^{-12} sec and a specific heat capacity of 7.0×10^{11} ergs/(g-eV). In this case, the unaccelerated spectral radius is approximately 0.53, and the accelerated spectral radius is approximately 0.26. As Figs. 1 and 2 suggest, both the unaccelerated and accelerated spectral radii change as a function of time step and heat capacity, but the shapes of $\omega_u(\lambda)$ and $\omega_a(\lambda)$ remain approximately invariant. The unaccelerated and accelerated spectral radii are given for several combinations of heat capacity and time step in Table 2. It can be seen that the unaccelerated spectral radius is very close to unity in most instances. Some perspective on the practical effect the acceleration scheme can be gained by noting that the error will be reduced by approximately an order of magnitude after a maximum of four iterations with a spectral radius of 0.57.

There are several fundamental characteristics of $\omega_a(\lambda)$ which are worth noting. First, $\omega_a(0)$ is zero. This is a direct consequence of the fact that the low-order operator becomes exact in the limit as λ approaches zero. Second, $\omega_a(\lambda)$ is positive for all λ and is strictly less than $\omega_u(\lambda)$. This means that every Fourier mode converges faster with the accelerated algorithm and, most importantly, that the accelerated spectral radius is always less than unity. Third, the accelerated spectral radius decreases as the multigroup equation becomes more "one-group-like." For instance, if the opacities and diffusion coefficients are identical for each group, the accelerated spectral radius is identically zero because the one-group operator is exact. There are many ways to measure the "closeness" of the multigroup equation to the one-group equation, and many distinct measures play a role in determining the accelerated spectral radius. For instance, if $\omega_u(\lambda)$ is expanded in a Taylor series about

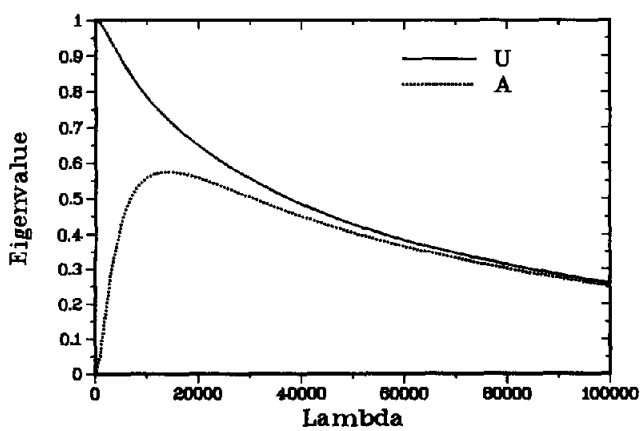

Fig. 2. Comparison of unaccelerated and accelerated eigenvalues for an infinite time-step.

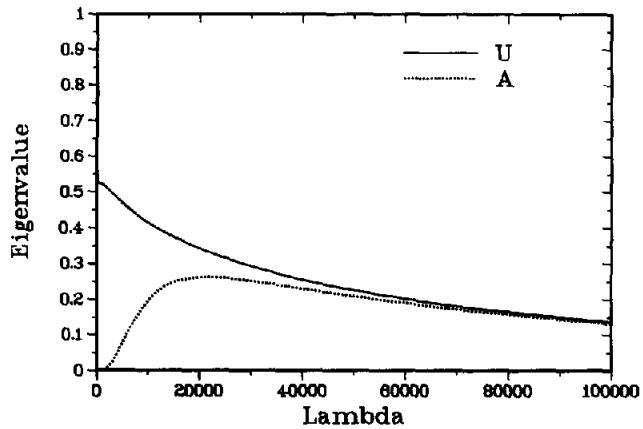

Fig. 3. Comparison of unaccelerated and accelerated eigenvalues for a finite time-step and a non-zero heat capacity.

zero, one finds that each expansion coefficient represents a measure of the energy variation of one or more quantities appearing in the multigroup equation. As an example, for the case of an infinite time-step,

$$\omega_a(\lambda) = \alpha\lambda^2 + O(\lambda^4) \quad , \tag{36}$$

where

$$\alpha = [\langle (D/\sigma_f)^2 \rangle - \langle D/\sigma_f \rangle^2]/\langle D/\sigma_f \rangle \quad , \tag{36a}$$

$$\langle D/\sigma_f \rangle = \sum_{n=1}^{NG} \chi_k D_k/\sigma_k \quad , \tag{36b}$$

$$\langle (D/\sigma_f)^2 \rangle = \sum_{n=1}^{NG} \chi_k (D_k/\sigma_k)^2 \quad . \tag{36c}$$

We now consider the relationship between the linear and nonlinear multifrequency-grey schemes. Although the two methods are quite distinct, there is a simple connection between them. However, it is difficult to see this connection unless both methods are cast in a nonstandard form. In particular, our method is formulated such that the accelerated intensities are obtained and then used to calculate the re-emission source. However, it is possible to reformulate it so as to directly solve for the accelerated re-emission source. The

Table 2. Parametric dependence of the unaccelerated and accelerated spectral radii.

Time Step (sec)	Heat Capacity (ergs/(g-eV))	Unaccelerated Spectral Radius	Accelerated Spectral Radius
1.0 E-10	1.0 E10	0.999	0.575
5.0 E-11	5.0 E10	0.994	0.570
1.0 E-11	1.0 E11	0.940	0.525
5.0 E-12	5.0 E11	0.609	0.308
1.0 E-12	1.0 E12	0.135	0.0623
1.0 E-10	1.0 E12	0.940	0.525
1.0 E-12	1.0 E10	0.940	0.522

connection between the linear and nonlinear schemes is most easily demonstrated when both schemes are formulated in this way. As an aid to interpreting certain quantities appearing in the alternate formulations, it is useful to consider first the exact equation for the re-emission source

$$-\nabla\cdot[\{\mathbf{D}\}\nabla(F/\{\sigma_f\}) + (\{\mathbf{D}'\}/\{\sigma_f\})F] + [\sigma_a/\{\sigma_f\} + 1 - \eta]F = S_0 \quad , \tag{37}$$

where

$$F = \sum_{g=1}^{NG} \sigma_{f,g} I_g \quad , \tag{37a}$$

$$S_0 = \sum_{g=1}^{NG} S_g \quad , \tag{37b}$$

$$\{\mathbf{D}\} = \left(\sum_{g=1}^{NG} \mathbf{D}_g I_g\right) \Big/ \left(\sum_{g=1}^{NG} I_g\right) \quad , \tag{37c}$$

$$\{\sigma_f\} = \left(\sum_{g=1}^{NG} \sigma_{f,g} I_g\right) \Big/ \left(\sum_{g=1}^{NG} I_g\right) \quad , \tag{37d}$$

$$\{\mathbf{D}'\} = \left\{\sum_{g=1}^{NG} \mathbf{D}_g \nabla\left[I_g \Big/ \left(\sum_{k=1}^{NG} I_k\right)\right]\right\} \quad . \tag{37e}$$

Equation (37) is obtained simply by first summing Eq. (20) over all groups to obtain an equation for the energy-integrated intensity, and then making the following substitution:

$$F/\{\sigma_f\} = \sum_{g=1}^{NG} I_g \quad . \tag{38}$$

Equation (37) is similar to our low-order equation in that it is a one-group equation derived from the multigroup equation under the assumption of a particular spectral shape. However, unlike our low-order equation, Eq. (37) is exact; but this is only true in a formal sense since knowledge of the exact spectral shape is required. Our low-order equation for the intensity errors, Eq. (34b), can be reexpressed, after a lengthy amount of algebra, to yield the accelerated re-emission source

$$-\nabla\cdot[\langle\mathbf{D}\rangle\nabla(F^{l+1}/\langle\sigma_f\rangle) + (\langle\mathbf{D}'\rangle/\langle\sigma_f\rangle)F^{l+1}] + [\sigma_a/\langle\sigma_f\rangle + 1 - \eta]F^{l+1} = S_0 + C^{l+\frac{1}{2}} \quad , \tag{39}$$

where

$$\begin{aligned} C^{l+\frac{1}{2}} = {} & \nabla\cdot[\{D\}^{l+\frac{1}{2}}\nabla(F^{l+\frac{1}{2}}/\{\sigma_f\}^{l+\frac{1}{2}}) - \langle\mathbf{D}\rangle\nabla(F^{l+\frac{1}{2}}/\langle\sigma_f\rangle)] \\ & + \nabla\cdot[(\{\mathbf{D}'\}^{l+\frac{1}{2}}/\{\sigma_f\}^{l+\frac{1}{2}})F^{l+\frac{1}{2}} - (\langle\mathbf{D}'\rangle/\langle\sigma_f\rangle)F^{l+\frac{1}{2}}] \\ & - (\sigma_a/\{\sigma_f\}^{l+\frac{1}{2}} - \sigma_a/\langle\sigma_f\rangle)F^{l+\frac{1}{2}} \end{aligned} \tag{39a}$$

and the spectrum-averaged quantities are defined as in Eqs. (37c)–(37e), except that the averaging is performed using the intensities at iteration step $l + \frac{1}{2}$, rather than the exact intensities. Inspection of Eq. (39) shows that it becomes equivalent to Eq. (37) upon

convergence of the intensities. Within this context, $C^{l+\frac{1}{2}}$ is seen to be a term which approximately corrects for the inaccuracy of the assumed infinite-medium spectrum using the spectral shape from iteration step $l + \frac{1}{2}$. Our scheme is linear because this correction term is additive. As an alternative to an additive correction term, one might simply employ the latest spectrum-averaged coefficients on the left hand side of Eq. (37):

$$-\nabla \cdot [\{\mathbf{D}\}^{l+\frac{1}{2}} \nabla (F^{l+1} / \{\sigma_f\}^{l+\frac{1}{2}}) + (\{\mathbf{D}'\}^{l+\frac{1}{2}} / \times \{\sigma_f\}^{l+\frac{1}{2}}) F^{l+1}] + [\sigma_a / \{\sigma_f\}^{l+\frac{1}{2}} + 1 - \eta] F^{l+1} = S_0 \quad . \tag{40}$$

Equation (40) can be thought of as being equivalent to Eq. (39) with multiplicative rather than additive correction factors. Specifically, Eq. (40) can be reexpressed as

$$-\nabla \cdot \{\langle \mathbf{D} \rangle \mathbf{C}_{\mathrm{d}}^{l+\frac{1}{2}} \nabla [F^{l+1} / (\langle \sigma_f \rangle C_f^{l+\frac{1}{2}})] + [\langle \mathbf{D}' \rangle \mathbf{C}_{\mathrm{d}}'^{l+\frac{1}{2}} / (\langle \sigma_f \rangle C_f^{l+\frac{1}{2}})] \times F^{l+1}\} + [\sigma_a / (\langle \sigma_f \rangle C_f^{l+\frac{1}{2}}) + 1 - \eta] F^{l+1} = S_0 \quad , \tag{41}$$

where

$$\langle \mathbf{D} \rangle \mathbf{C}_{\mathrm{d}}^{l+\frac{1}{2}} = \{\mathbf{D}\}^{l+\frac{1}{2}} \quad , \tag{41a}$$

$$C_f^{l+\frac{1}{2}} = \{\sigma_f\}^{l+\frac{1}{2}} / \langle \sigma_f \rangle \quad , \tag{41b}$$

$$\langle \mathbf{D}' \rangle \mathbf{C}_{\mathrm{d}}'^{l+\frac{1}{2}} = \{\mathbf{D}'\}^{l+\frac{1}{2}} \quad . \tag{41c}$$

Although in a nonstandard form, use of Eq. (41) to obtain the accelerated re-emission source is equivalent to the standard nonlinear multifrequency-grey method. Thus we see that the linear and nonlinear methods differ only in that additive or linear correction factors are used in the former, while multiplicative or nonlinear correction factors are used in the latter. The similarity between the two methods becomes even more striking when one considers that both the linearly and nonlinearly accelerated re-emission sources can be shown to satisfy (after a great deal of algebra for the linear case)

$$-\nabla \cdot [\{\mathbf{D}\}^{l+1} \nabla (F^{l+1} / \{\sigma_f\}^{l+1}) + (\{\mathbf{D}'\}^{l+1} / \times \{\sigma_f\}^{l+1}) F^{l+1}] + [\sigma_a / \{\sigma_f\}^{l+1} + 1 - \eta] F^{l+1} = S_0 \quad . \tag{42}$$

This result would seem to indicate that the two methods are equivalent, but it must be remembered that the spectral shapes (and hence the spectrum-averaged coefficients) at iteration steps $l + \frac{1}{2}$ and $l + 1$ differ in the linear scheme, but are identical in the nonlinear scheme. Thus, while Eq. (42) is satisfied with both methods, the coefficients appearing in the equation differ in the two cases. Although it may not be obvious, Eq. (40) expresses the local conservation of total photon energy. Thus both the linearly and nonlinearly accelerated iterates exhibit local energy conservation after each iteration, whereas the standard unaccelerated iterate does not.

A computational comparison of the linear and nonlinear multifrequency-grey methods is beyond the scope of this paper. However, as previously noted, experience with similarly related linear and nonlinear synthetic acceleration schemes for the discrete-ordinates equations indicates that they are essentially equivalent in terms of the number of iterations required to converge the solution. Preliminary results from a comparative study of the linear and nonlinear multifrequency-grey methods confirm these expectations.[10]

For simplicity, we have thus far assumed a continuous spatial dependence in the multigroup diffusion equation. The extension of our method for the case of a discrete spatial dependence is straightforward, but caution must be exercised. It was found in early discrete-ordinates applications of the synthetic method that schemes, which were shown through Fourier analysis to be very effective under the assumption of a continuous spatial dependence, often became unstable in the discrete case when large (optically thick) mesh cells were used. The source of this difficulty was eventually found to be subtle inconsistencies between the

discrete forms of the high-order and low-order operators. Furthermore, it was found that these inconsistencies could be avoided if the discretized low-order operator was derived directly from the discretized high-order operator, rather than being obtained from an arbitrary discretization of the continuous low-order operator. In keeping with this result, we derive our discretized one-group operator directly from the discretized multigroup operator. The procedure employed is applicable with any kind of spatial differencing scheme. We demonstrate the procedure in detail for the one-dimensional center-differenced multigroup diffusion equation.

The first half of the iteration algorithm is defined by the discretized version of Eq. (34a)

$$
\begin{aligned}
&-\frac{D_{k,i+\frac{1}{2}}}{\Delta x_{i+\frac{1}{2}}}\left(I_{k,i+1}^{l+\frac{1}{2}}-I_{k,i}^{l+\frac{1}{2}}\right)+\frac{D_{k,i-\frac{1}{2}}}{\Delta x_{i-\frac{1}{2}}}\left(I_{k,i}^{l+\frac{1}{2}}-I_{k,i-1}^{l+\frac{1}{2}}\right)\\
&+\left(\sigma_a+\sigma_{f,k,i}\right)I_{k,i}^{l+\frac{1}{2}}\Delta x_i \qquad (43)\\
&=\eta_i\chi_{k,i}\sum_{g=1}^{NG}\sigma_{f,g,i}I_{g,i}^{l}\Delta x_i+S_{k,i}\Delta x_i \quad ,
\end{aligned}
$$

where

$$\Delta x_i=x_{i+\frac{1}{2}}-x_{i-\frac{1}{2}} \quad , \qquad (43a)$$

$$\Delta x_{i+\frac{1}{2}}=x_{i+1}-x_i \quad , \qquad (43b)$$

$$D_{k,i+\frac{1}{2}}=2\Delta x_{i+\frac{1}{2}}\left[\Delta x_{i+1}/D_{k,i+1}+\Delta x_i/D_{k,1}\right]_i^{-1} \quad . \qquad (43c)$$

The spatial index in Eq. (43) is i. Integral values of i denote cell-center quantities, and half-integral values denote cell-edge quantities. The exact equation for the intensity iterate errors corresponding to Eq. (43) is

$$
\begin{aligned}
&-\frac{D_{k,i+\frac{1}{2}}}{\Delta x_{i+\frac{1}{2}}}\left(\epsilon_{k,i+1}^{l+\frac{1}{2}}-\epsilon_{k,i}^{l+\frac{1}{2}}\right)+\frac{D_{k,i-\frac{1}{2}}}{\Delta x_{i-\frac{1}{2}}}\left(\epsilon_{k,i}^{l+\frac{1}{2}}-\epsilon_{k,i-1}^{l+\frac{1}{2}}\right)\\
&+\left(\sigma_{a,i}+\sigma_{f,k,i}\right)\epsilon_{k,i}^{l+\frac{1}{2}}\Delta x_i \qquad (44)\\
&=\eta_i\chi_{k,i}\sum_{g=1}^{NG}\sigma_{f,g,i}\left(\epsilon_{g,i}^{l+\frac{1}{2}}+I_{g,i}^{l+\frac{1}{2}}-I_{g,i}^{l}\right)\Delta x_i \quad .
\end{aligned}
$$

The discrete low-order equation is derived from Eq. (44) in exactly the same way that the continuous low-order operator is derived from Eq. (29). It is easily shown that the infinite-medium solution to Eq. (44) has the form

$$\epsilon_{k,i}^{l+\frac{1}{2}}=E_i^{l+\frac{1}{2}}\langle\sigma_{t,i}\rangle\chi_i/\sigma_{t,k,i} \quad . \qquad (45)$$

Substituting Eq. (45) into Eq. (44) and summing over all groups yields the desired equation:

$$
\begin{aligned}
&-\left(\frac{\langle D_{i+1}^{-}\rangle}{\Delta x_{i+\frac{1}{2}}}E_{i+1}^{l+\frac{1}{2}}-\frac{\langle D_i^{+}\rangle}{\Delta x_{i+\frac{1}{2}}}E_i^{l+\frac{1}{2}}\right)+\left(\frac{\langle D_i^{-}\rangle}{\Delta x_{i-\frac{1}{2}}}E_i^{l+\frac{1}{2}}-\frac{\langle D_{i-1}^{+}\rangle}{\Delta x_{i-\frac{1}{2}}}E_{i-1}^{l+\frac{1}{2}}\right)\\
&+\left[\sigma_{a,i}+(1-\eta)\langle\sigma_{f,i}\rangle\right]E_i^{l+\frac{1}{2}}\Delta x_i \qquad (46)\\
&=\eta_i\sum_{g=1}^{NG}\sigma_{g,i}\left(I_{g,i}^{l+\frac{1}{2}}-I_{g,i}^{l}\right)\Delta x_i \quad ,
\end{aligned}
$$

where

$$\langle D_i^- \rangle = \langle \sigma_{t,i} \rangle \sum_{g=1}^{NG} D_{g,i-1/2} \chi_{g,i} / \sigma_{t,g,i} \quad , \tag{46a}$$

$$\langle D_i^+ \rangle = \langle \sigma_{t,i} \rangle \sum_{g=1}^{NG} D_{g,i+1/2} \chi_{g,i} / \sigma_{t,g,i} \quad . \tag{46b}$$

In accord with Eq. (45), the discrete accelerated intensities are

$$I_{k,i}^{l+1} = I_{k,i}^{l+1/2} + E_i^{l+1/2} \langle \sigma_{t,i} \rangle \chi_{k,i} / \sigma_{t,k,i} \quad . \tag{47}$$

Assuming an infinite uniform mesh, a Fourier analysis can be performed for the discrete scheme which is completely analogous to the analysis for the continuous case. We simply assume that

$$I_{k,i} = I_k e^{j\lambda x_i}, \quad -\infty < \lambda < +\infty \quad . \tag{48}$$

The unaccelerated and accelerated eigenvalues for the discrete case are respectively given by

$$\omega_u(\lambda) = \eta \sum_{g=1}^{NG} [\chi_g \sigma_{f,g}] / [D_g \lambda_d^2 + \sigma_a + \sigma_{f,g}] \quad , \tag{49}$$

where

$$\lambda_d^2 = [1.0 - \cos(\lambda \Delta x)] 2/(\Delta x)^2 \quad , \tag{49a}$$

and

$$\omega_a(\lambda) = \omega_u(\lambda) + [\omega_u(\lambda) - 1.0] \langle \sigma_f \rangle / [\langle D \rangle \lambda^2 + \sigma_a + (1 - \eta) \langle \sigma_f \rangle] \quad . \tag{50}$$

It is important to note that Eqs. (49) and (50) become identical to their continuous-case counterparts if λ_d^2 is replaced with λ^2. A Taylor-series expansion of λ_d^2 gives

$$\lambda_d^2 = \lambda^2 - (\Delta x)^2 \lambda^4 / 12 + O(\lambda^6) \quad . \tag{51}$$

As one would expect, Eq. (51) shows that the continuous and discrete cases become equivalent in the limit as the cell width becomes small with respect to the wavelength of a mode. Inspection of Eq. (49a) shows that λ_d^2 is an even and periodic function of λ having a minimum value of zero and a maximum value, $\lambda_{max}^2 = 4/(\Delta x)^2$. As the cell width is increased, λ_{max}^2 converges to zero, and the unaccelerated eigenvalues uniformly converge to unity. Since our acceleration method becomes exact in the limit as λ_d^2 goes to zero, it follows that the accelerated eigenvalues converge to zero as the cell width is increased. This result is a direct consequence of the fact that local thermodynamic equilibrium is attained in optically-thick systems. To demonstrate the effect of cell width, we plot the accelerated and unaccelerated eigenvalues for the model opacities with an infinite time-step and cell widths of 10^{-5} g/cm^2 (approximately 0.1 equilibrium-averaged mean-free-paths) and 10^{3} g/cm^2 (approximately 10 equilibrium-averaged mean-free-paths) in Figs. 4 and 5, respectively. Since the functions are periodic and even, only a half period is plotted. The spectral radius for the optically-thin case is identical to the continuous-case spectral radius, but the spectral radius for the optically-thick case is significantly less. In general, the spectral radii for the continuous and discrete cases will be identical if the cell width is sufficiently small, otherwise the discrete-case spectral radius will be less than the continuous-case spectral radius.

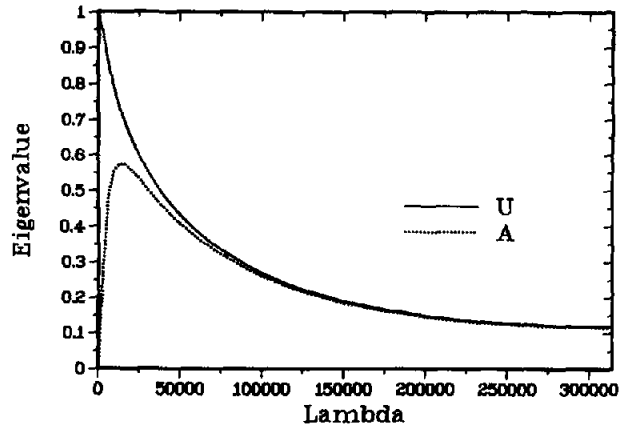

Fig. 4. Comparison of unaccelerated and accelerated eigenvalues for an infinite time-step and optically-thin cells (discrete spatial treatment).

COMPUTATIONAL RESULTS

In this section we give computational results for a simple but realistic problem consisting of a 200-μm-thick iron slab with a uniformly distributed energy source of 1.31×10^{22} ergs/(g-sec). The initial density of the slab is 0.786 g/cm^3 (0.1 standard density) and the initial temperature is 1 eV. This source results in a maximum equilibrium temperature of approximately 140 eV. A total of four calculations were performed for this problem, corresponding to the use of the accelerated and unaccelerated iteration schemes with both 10 and 100 spatial zones, respectively. In order to insure a valid test of the theoretical results relating to the effect of cell thickness, hydrodynamics was not performed. However, thermal conductivity was included. The source was set to zero in the calculations after a period of 10 ns, at which point the system was essentially in equilibrium. The system was then allowed to relax for another two nanoseconds, after which the calculations were terminated. A total of 169 time-steps were required to complete each calculation. The radiation intensity and material-temperature solutions from each of the calculations were nearly identical even though the cell widths varied by a factor of ten. This means that temperature-dependent quantities such as the heat capacity and opacities were essentially the same in all of the calculations. Such invariance is required to maintain consistency between the theoretical analysis and the calculations. At equilibrium, the cell widths for the 100- and 10-zone calculations were approximately 0.5 and 5.0 equilibrium-averaged mean-free-paths, respectively. The solution at each time-step was considered converged when the maximum absolute value of the relative change in the re-emission source was less than 10^{-4} in each cell, i.e.

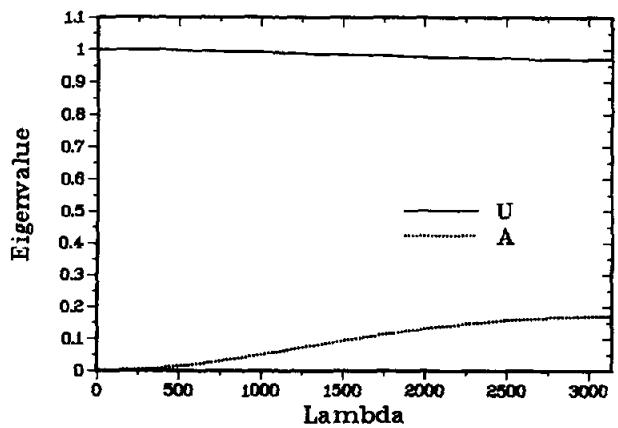

Fig. 5. Comparison of unaccelerated and accelerated eigenvalues for an infinite time-step and optically-thick cells (discrete spatial treatment).

Table 3. A computational comparison of the unaccelerated and accelerated algorithms.

Iteration Method	Number of Cells	Total Iterations
Unaccelerated	10	4357
Accelerated	10	361
Unaccelerated	100	4368
Accelerated	100	560

$$|(F^{l+1} - F^l)/F^{l+1}| < 10^{-4} \quad , \tag{52}$$

where F is given by Eq. (37a). The time step was restricted in accordance with Eqs. (19)–(19b) using $\alpha = 0.1$. The opacity set that was used is the same set from which the model opacities were taken. The equation-of-state data was taken from the SESAME[11] tables developed at Los Alamos National Laboratory.

Results from the calculations are given in Table 3. As expected, the acceleration scheme is quite effective. Furthermore, the scheme is substantially more effective in the 10-zone case than in the 100-zone case. This is in agreement with the theoretical analysis. Although we have presented detailed results here for only a single problem, we have performed hundreds of realistic calculations using our acceleration technique, and have so far observed no anomalous behavior. Thus the theoretical results appear to be valid for realistic as well as idealized calculations.

CONCLUSIONS

We have developed a synthetic acceleration scheme for radiative diffusion calculations, which appears to be quite effective. The method has been extensively characterized in terms of a Fourier analysis. The standard nonlinear multifrequency-grey technique is related to our linear synthetic method, but is quite distinct. However, preliminary testing indicates that they can be expected to be roughly equivalent in terms of the number of iterations required to converge the solution. Furthermore, when cast in similar forms, the computational work required by the methods is essentially equal. The question arises as to which method should be used. In calculations of a novel nature, we would feel safer with the linear scheme because its performance can be predicted on the basis of a Fourier analysis. However, it is conceivable that there may be certain types of problems where the nonlinear method performs better. Thus computational comparisons of the two methods for a wide variety of problems should be performed in the future.

We have recently begun to investigate extensions of our method based upon the use of more accurate low-order operators. The accelerated spectral radius can be significantly reduced with such operators, but higher efficiency is not necessarily obtained because of the increase in computational cost associated with solving a more complicated set of low-order equations. Such extensions of our method should continue to be investigated in the future.

Acknowledgements—This work was performed at Sandia and Los Alamos National Laboratories and was supported by the U.S. Department of Energy under Contract Nos. DE-AC04-76DP00789 and W-7405-ENG-36, respectively.

REFERENCES

1. E. M. Lund and J. R. Wilson, unpublished Report UCRL-84678. Lawrence Livermore National Laboratory, Livermore, California (July 1980).
2. E. M. Gelbard and L. A. Hageman, *Nucl. Sci. Eng.* **37**, 208 (1969).
3. W. H. Reed, *Nucl. Sci. Eng.* **45**, 245 (1971).
4. R. E. Alcouffe, *Nucl. Sci. Eng.* **64** 344 (1977).
5. J. E. Morel, *Nucl. Sci. Eng.* **82**, 34 (1982).

6. E. W. Larsen, *Nucl. Sci. Eng.* **82**, 47 (1982).
7. G. C. Pomraning, *Radiation Hydrodynamics*. Pergamon Press, New York (1973).
8. W. F. Hubner, A. L. Merts, N. H. Magee and M. F. Argo, Report LA-6760-M. Los Alamos National Laboratory, Los Alamos, New Mexico (1977).
9. E. W. Larsen, Progress Report LA-9451-PR. (Edited by R. D. O'Dell and R. E. Alcouffe), p. 45. Los Alamos National Laboratory, Los Alamos, New Mexico (August 1982).
10. R. E. Alcouffe, B. A. Clark and E. W. Larsen, The Diffusion Synthetic Acceleration of Transport Iterations with Application to a Radiation-Hydrodynamics Problem, in Multiple Time Scales (Edited by J. Brackbill and B. Cohen). Academic, New York (to be published).
11. B. I. Bennett, J. D. Johnson, G. I. Kerley and G. T. Rood, unpublished Report LA-7130, Los Alamos National Laboratory, Los Alamos, New Mexico (February 1978).